

Interplay of rheology and entrainment in debris avalanches: a numerical study

Sabatino Cuomo, Manuel Pastor, Leonardo Cascini, and Giuseppe Claudio Castorino

Abstract: Flow-type landslides are a major global hazard. They occur worldwide, and are responsible for a large number of casualties, significant structural damage to property and infrastructure, and economic losses. The features of debris avalanches are particularly important, as they involve open slopes and affect triangular source areas when initial slides turn into avalanches through further failures or eventual soil entrainment. In this paper, the propagation stage of debris avalanches is numerically modelled to provide information such as the propagation pattern of the mobilized material and its velocity, thickness, and run-out distance. The use of a “depth-integrated” model has the following advantages: (i) it adequately accommodates the irregular topography of real slopes, which greatly affects the evolution of the propagation stage; and (ii) it is less time consuming than full three-dimensional approaches. The model is named “GeoFlow_SPH” and has previously been applied to theoretical, experimental, and real case histories. The behaviour of debris avalanches is analysed with particular attention to the apical angle, one of the main features of this type of landslide, in relation to soil rheology, hillslope geometry, and the geometric aspect ratio of the triggering area. The role of bed entrainment is also investigated with reference to differences in steepness of the uppermost parts of open slopes. First, simplified benchmark slopes are analysed using both water-like materials (with negligible shear strength) and debris-type materials (saturated frictional soil). Next, the paper addresses three important case studies from the Campania region of southern Italy (Cervinara, Nocera Inferiore, and Sarno), where debris avalanches occur in pyroclastic soils that originated from the eruptive products of the Mount Vesuvius volcano. In all of the cases analysed, the effects of erosion rate are compared with those of simulated soil propagation height, run-out distance, and velocity. In a novel contribution to the existing research, the results obtained from analysis of both the benchmark slopes and the real case histories indicate that landslide propagation depends on the interplay of rheology and bed entrainment. In particular, increased erosion growth rates correspond to shorter run-out distances, lower velocities, and larger propagation depths. It is further shown that erosion depth increases with either friction angle or the consolidation coefficient of pore-water pressure; the latter reduces bed entrainment but does not significantly affect the apical angle of debris avalanches. Globally, the results are particularly satisfactory because they indicate that the GeoFlow_SPH model is a suitable tool for the analysis and forecasting of debris avalanches.

Key words: landslide, modelling, numerical, smoothed particle hydrodynamics (SPH), entrainment.

Résumé : Les glissements de terrain de type écoulement sont un danger global majeur. Ils se produisent à la grandeur de la planète, et sont responsables d'un grand nombre de pertes de vies humaines, de dommages structuraux significatifs à la propriété et aux infrastructures, et de pertes économiques. Les caractéristiques des avalanches de débris sont particulièrement importantes, puisqu'elles impliquent des pentes ouvertes et affectent des zones de sources triangulaires lorsque les glissements initiaux deviennent des avalanches via d'autres ruptures ou l'entraînement du sol. Dans cet article, l'étape de propagation des avalanches de débris est modélisée numériquement afin de fournir de l'information comme le patron de propagation du matériel mobilisé et sa vitesse, épaisseur et distance d'écoulement. L'utilisation d'un modèle « profondeur intégrée » offre les avantages suivants : (i) il représente adéquatement la topographie irrégulière des pentes réelles, ce qui affecte grandement l'évolution de l'étape de propagation; et (ii) il est plus rapide que les approches tridimensionnelles complètes. Le modèle est nommé « GeoFlow_SPH » et a été utilisé précédemment pour des cas théoriques, expérimentaux et réels. Le comportement des avalanches de débris est analysé avec une attention particulière à l'angle au sommet, une des principales caractéristique de ce type de glissement de terrain, en lien avec la rhéologie du sol, la géométrie des pentes, et le rapport de longueur géométrique de la zone de déclenchement. Le rôle de l'entraînement du lit est aussi étudié en référence aux différences d'inclinaison dans les parties supérieures des pentes ouvertes. Premièrement, des pentes témoins simplifiées sont analysées avec des matériaux semblables à l'eau (avec une résistance au cisaillement négligeable) et des matériaux de type débris (sol frictionnel saturé). Ensuite, l'article discute trois études de cas importantes de la région de Campania au sud de l'Italie (Cervinara, Nocera Inferiore et Sarno), où des avalanches de débris se produisent dans des sols pyroclastiques qui proviennent des produits d'éruption du volcan du Mont Vésuve. Dans tous les cas analysés, les effets du taux d'érosion sont comparés aux taux simulés de hauteur de propagation du sol, de distance d'écoulement et de vitesse. En tant que nouvelle contribution à la recherche existante, les résultats obtenus de l'analyse des pentes témoins et des études de cas réels indiquent que la propagation des glissements de terrain dépend de l'interaction de la rhéologie et de l'entraînement du lit. Plus particulièrement, l'augmentation des taux d'érosion correspond à des distances d'écoulement plus courtes, des vitesses plus faibles et des profondeurs de propagation plus grandes. Il est aussi démontré que la profondeur d'érosion augmente avec soit l'angle de friction ou le coefficient de consoli-

Received 10 October 2013. Accepted 29 April 2014.

S. Cuomo, L. Cascini, and G.C. Castorino. Laboratory of Geotechnics, Department of Civil Engineering, University of Salerno, Via Ponte Don Melillo 1, 84084 Fisciano (SA), Italy.

M. Pastor. Department of Applied Mathematics and Computer Science, ETS Ingenieros de Caminos, Universidad Politecnica de Madrid, Madrid, Spain.

Corresponding author: Sabatino Cuomo (e-mail: scuomo@unisa.it).

tion de la pression interstitielle; ce dernier réduit l'entraînement du lit mais n'affecte pas significativement l'angle au sommet des avalanches de débris. Globalement, les résultats sont particulièrement satisfaisants puisqu'ils indiquent que le modèle GeoFlow_SPH est un outil adéquat pour l'analyse et la prédiction des avalanches de débris. [Traduit par la Rédaction]

Mots-clés : glissement de terrain, modélisation, numérique, hydrodynamique des particules lissée (SPH), entraînement.

Introduction

Flow-type landslides (Hungri et al. 2001, 2014) are a global hazard responsible for large numbers of casualties and widespread damage, as they travel long distances at extremely rapid velocities, and can affect large areas at the piedmonts of hillslopes, which provide favourable conditions for urban development and are thus often settled. In their classification of landslides, Hungri et al. (2001) define debris avalanches as “very rapid to extremely rapid shallow flows of partially or fully saturated debris on a steep slope, without confinement in an established channel”. Debris avalanches merit special attention for the following distinctive features: (i) they affect open slopes, that is, shallow soil deposits with nearly constant depths and slope angles generally between 30° and 45°; (ii) they originate as small landslides (the failure stage) involving 1–2 m thick deposits of coarse-grained and cohesionless soils; and (iii) their initial volumes increase in triangular areas (the post-failure stage) by means of complex mechanisms (Chen et al. 2006; Crosta et al. 2006; Cascini et al. 2013a). The focus of this paper is debris avalanches involving coarse-grained soils, that is, sands and gravels, of which typical examples are found in torrent deposits in the USA (Costa and Williams 1984), decomposed granitic soils in Japan (Wang et al. 2003), pyroclastic deposits in southern Italy (Revellino et al. 2004; Cascini et al. 2008), debris deposits in Valtellina (northern Italy) (Chen et al. 2006) and colluvial soils in British Columbia (Hungri et al. 2008). Regardless of environmental context, debris avalanches always form a distinctive triangular shape, rather like snow avalanches (Jamieson and Stethem 2002, among others). They are generally <200 m in width, with an uppermost zone of a few metres, and the lengths of their source areas vary from 300 to 500 m. The volumes involved range from a few hundred cubic metres to several tens of thousands of cubic metres (Hungri et al. 2008). In some cases, debris avalanches also involve rocks and boulders, but this phenomenon is not analysed in this paper.

The advanced numerical modelling of debris avalanches may provide a valuable tool for the following purposes: (i) improving the understanding of the inception of debris avalanches (i.e., their triggering mechanisms and avalanche formation); (ii) evaluating the volume mobilized inside the avalanche source area, which is crucial to hazard and risk assessment and zoning; and consequently (iii) improving the ability to accurately forecast the features of this type of landslide.

This paper contributes to existing research on this topic by analysing the propagation stage of debris avalanches, with particular attention to the interplay of material rheology and bed entrainment. First, benchmark cases with water-like materials and mixed water and frictional materials (fully or partially saturated) are analysed. Next, three relevant case studies from the Campania region of southern Italy are selected and simulated to provide a wide range of event scenarios, such as (i) the cessation of the 2005 Nocera Inferiore debris avalanche at the toe of the hillslope, (ii) the evolution of the 1998 Sarno debris avalanche in two channelised debris flow paths, and (iii) the run-up of the 1999 Cervinara debris avalanche on the opposite slope, with the failed mass later channelising within the main valley. To this end, the depth-integrated “GeoFlow_SPH” model (SPH, smoothed particle hydrodynamics; Pastor et al. 2009) is used to simulate both propagation and entrainment phenomena using the empirical erosion law proposed by McDougall and Hungri (2005). Finally, the results are used to offer insights into the run-out distances,

propagation patterns, and bed entrainment of debris avalanches. In particular, it is shown that landslide propagation depends on the interplay of rheology and bed entrainment, erosion depths increase with either friction angle or consolidation coefficient, and bed entrainment is reduced by pore-water pressure.

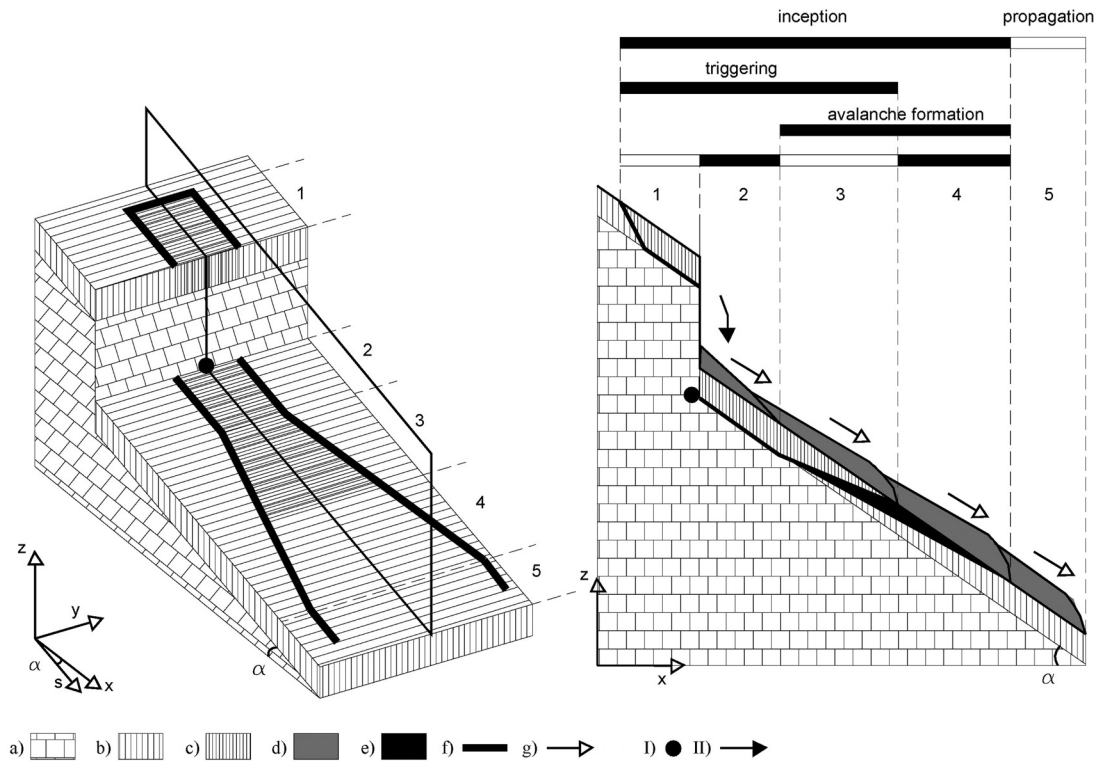
Literature review

The peculiarities of debris avalanches have for many years motivated extensive research activities designed to improve the understanding and (or) characterization of debris avalanches and the modelling of real events and field evidence.

With regard to the characterization of debris avalanches, many studies have shown that the amount of entrained material can reach 40% of the volume triggered in the source area(s) (Cascini 2004, 2005) or more (Revellino et al. 2004). Variation in the apical angles of debris avalanches (i.e., the angle between the lateral boundaries of the source area) has also been investigated (Di Crescenzo and Santo 2005), and fairly weak correlations have been found between the apical angle and the morphometric features of a hillslope, and between the apical angle and soil-cover thickness. Experimental studies conducted by Daerr and Douady (1999), Bowman et al. (2012), Manzella and Labiouse (2009), and Crosta et al. (2006) found that loading perturbation in a thin layer causes avalanches to propagate downhill and laterally owing to collisions between neighbouring grains, resulting in triangular tracks, whereas loading perturbation in a thick layer creates an avalanche front that propagates upwards. Extensive research has been conducted on snow avalanches, which characteristically spread out into the shape of an inverted “V”, especially within cohesionless near-surface layers of newly fallen snow or within the wet surface snow that results from melt (Jamieson and Stethem 2002; Pielmeier and Schneebeli 2003). Sovilla and Bartelt (2002), among others, highlight the importance of entrainment to the formation of snow avalanches through extensive in situ measurements of snow-avalanche heights in certain areas of Switzerland. Naaim et al. (2004) address both lateral spreading and entrainment using a frictional approach with satisfactory matching between theoretical and observed run-out and mobilized volumes.

More recently, Cascini et al. (2013a) distinguished between two stages in the inception of debris avalanches: the failure stage and the avalanche-formation stage. The former comprises all of the triggering mechanisms that cause the soil to fail; the latter is associated with an increase in unstable volume. Five zones can be identified within these stages (Fig. 1). Zone 1 corresponds to small failures that occur at natural or anthropogenic discontinuities in soil deposits (respectively, bedrock outcrops and cut slopes). Zone 2 is the impact zone of the previously mentioned failed masses. This zone usually corresponds to water supplies from bedrock (either karst springs or water runoff at bedrock outcrops). In the absence of zone 1, zone 2 is the source area for small landslides triggered by water supplies from the bedrock. Zone 3 corresponds to two distinct mechanisms: the thrust of the failed mass on downslope stable material, and soil entrainment caused by the propagating mass. Zone 4 corresponds exclusively to soil entrainment. It is worth noting that whereas zones 1 and 2 are a few tens of metres in size, the widths of zones 3 and 4 are not known a priori, which makes it difficult to forecast their features. Zone 5 corresponds to propagation. The framework proposed for debris avalanches by Cascini et al. (2013a) is used in this paper with

Fig. 1. Reference scheme for debris avalanches: (a) bedrock; (b) stable soil deposit; (c) failed soil; (d) propagating failed mass; (e) entrained material; (f) boundary of debris avalanche; (g) propagation pattern (Cascini et al. 2013a). I, spring from bedrock; II, impact loading; s, axis along the slope; α , angle of reach.



particular attention to zones 3–5, assuming a soil volume but without analysis of its triggering mechanism.

Both discrete and continuum soil mechanics have been used to model the propagation stage of debris avalanches (e.g., Calvetti et al. 2000; Fannin and Wise 2001; Pastor et al. 2002, 2004; Hungr and McDougall 2009; Viccione and Bovolin 2011). In principle, discrete modelling is the best method for analysing the kinematics of granular media, and satisfactory back-analyses have been proposed, in particular for dry debris avalanches observed in the Italian Alps (Calvetti et al. 2000) and Switzerland (McDougall and Hungr 2004). However, discrete approaches that accommodate the effects of pore-water pressure (Catalano et al. 2011, 2014) are rarely used to model real case histories because they are extremely time consuming. McDougall and Hungr (2005) use a continuum-based approach to simulate reduced-scale tests of a 1 m long, 45°-inclined plane with and without an erodible zone in the middle of its slope. Their findings indicate that entrainment modifies the pattern of avalanche propagation. Pirulli and Pastor (2012) emphasise the importance of correctly simulating channel material entrainment during the propagation stage when analysing rapid landslides. However, most available approaches handle the heterogeneous and multiphase moving mass of a debris avalanche as a single-phase continuum. Conversely, Pastor et al. (2007) and Cascini et al. (2013a) use a continuum-based (depth-integrated) hydromechanical coupled SPH model to simulate debris avalanches and test the relative effects of pore-water pressure consolidation and material entrainment along the propagation path. Their findings indicate that both factors are related to the lateral spreading of the unstable mass, and that they also control the kinematic features of landslides, such as the propagation height and velocity. It is worth mentioning that also bed deformation may modify pore pressure during flow propagation (Iverson 2012).

The literature provides extensive insights into the behaviour of debris avalanches, and several alternatives for modelling. The analysis of benchmark tests and real case histories is the most straightforward method of evaluating the potential efficacy and limitations of existing numerical tools.

Remarks on modelling of debris avalanches

Chosen model

The GeoFlow_SPH model proposed by Pastor et al. (2009) is used in this paper. The model is based on a theoretical framework proposed by Hutchinson (1986) and Pastor et al. (2002), and schematizes the propagating mass as a solid–fluid mixture comprising a solid skeleton saturated with water. The unknowns are the velocity of the solid skeleton (v) and the pore-water pressure (p_w).

The governing equations are as follows: (i) the balance of mass of the mixture combined with the balance of linear momentum of the pore fluid; (ii) the balance of the linear momentum of the mixture; (iii) a rheological equation relating the soil-stress tensor to the deformation-rate tensor; and (iv) a kinematic relation between the deformation-rate tensor and velocity field, also known as the “rheological law”. It is assumed that pore-water pressure dissipation takes place in the normal direction to the ground surface (one-dimensional consolidation) during the propagation stage. At this point, a propagation–consolidation model can be derived by regarding the velocity of the solid skeleton and pressure fields as the sum of two components, respectively, related to propagation and consolidation. As many flow-type landslides have small average depths compared with their lengths or widths, these equations can be integrated along the vertical axis. The resulting two-dimensional depth-integrated model offers both simplicity and a high level of accuracy. The GeoFlow_SPH model also accounts for bed entrainment along the landslide path, and the elevation of ground surface consistently decreases in time.

The entrained material is assumed to have nil velocity and nil pore-water pressure when entrained by the propagating mass. The erosion rate (e_r) is defined as a time derivative of the ground-surface elevation, and is equal to the time derivative of the soil depth of the propagating mass when other causes are not in play. The erosion rate is assumed to be equal to the product of three terms, as shown in eq. (1): the “landslide growth rate” (E_r), which is independent of flow velocity; propagation height (h); and flow velocity (v).

$$(1) \quad e_r = E_r h v$$

Once E_r has been assigned, the amount of bed entrainment — the cumulative value of the erosion rate over time, or eroded depth (h_{er}) — depends on both the height and velocity of the propagating mass and the time duration of the flow at each point on the landslide path. The GeoFlow_SPH model contains various empirical laws governing the landslide growth rate (E_r), such as the laws proposed by Hungr (1995), Egashira et al. (2001a, 2001b), McDougall and Hungr (2005), and Blanc et al. (2011). These laws have been also tested using real case studies (Pastor et al. 2007, 2010; Blanc et al. 2011; Sánchez et al. 2013). The simple yet effective law proposed by McDougall and Hungr (2005) is used in the following sections, primarily to achieve results comparable with those of most previous studies. The sensitivity of the model to landslide growth rate is investigated by changing this input within a wide range of values suggested by the literature. In particular, McDougall and Hungr (2005) relates landslide growth rate (E_r) to initial landslide volume ($V_{initial}$) and final landslide volume (V_{final}), and to the distance travelled (L), as follows:

$$(2) \quad E_r = \frac{\ln(V_{final}/V_{initial})}{L}$$

The GeoFlow_SPH model uses a SPH method that discretizes the propagating mass into a set of moving “particles” or “nodes”. Information such as unknowns and their derivatives is linked to the particles. The SPH discretization is carried out using a set of ordinary differential equations, and the accuracy of the numerical solution and the level of approximation for engineering purposes depend on how the nodes are spaced (Cuomo et al. 2013). However, slope topography is represented by a digital terrain model (DTM), consisting of a mesh of as many square elements as is necessary to gain a detailed description of the ground surface without any additional effort (Cuomo et al. 2013). In other words, the SPH computational nodes are independent of the elements of the DTM mesh.

Interested readers can find the details of this mathematical and numerical model in Pastor et al. (2009) and Blanc et al. (2011). For the sake of clarity, the governing equations are provided here to illustrate the relationship between the basal-resistance and pore-pressure terms and the entrainment term, which has an important influence on the lateral spreading. Specifically, a depth-averaged model is obtained by integrating the balance of mass and momentum equations along depth (hereafter x_3). The following is obtained from the balance of mass equation:

$$(3) \quad \frac{dh}{dt} + h \operatorname{div}(\bar{v}) = e_r$$

where e_r is the erosion rate [$L T^{-1}$], h is the soil depth, t is time, and \bar{v} is the depth-averaged velocity given by

$$(4) \quad \bar{v} = \frac{1}{h} \int_0^h v \, dx_3$$

Similarly, the balance of linear momentum equation first yields the following result:

$$(5) \quad \rho \frac{d\bar{v}}{dt} = \frac{1}{2} \rho \operatorname{grad}(h^2 b_3) + \rho h b_3 \operatorname{grad}(Z) - \tau_b + \rho b h - e_r \bar{v}$$

where ρ is the density of the solid-pore-fluid mixture; b denotes the gravity force components along depths x_1 and x_2 , and b_3 denotes the gravity forces along x_3 ; Z is the ground-surface elevation; and τ_b is the basal shear stress, which is determined by a suitable rheological model. In the case of pure frictional fluids, the momentum equation gives the following result.

$$(6) \quad \tau_b = [(\rho_s - \rho_w)(1 - n)h b_3 - p_{wb}] \frac{\bar{v}}{|\bar{v}|} \tan \phi_b$$

where ϕ_b is the basal friction angle; n is the porosity; ρ_s and ρ_w are the densities of the solid particles and the pore fluid, respectively; and p_{wb} is the basal pore pressure.

The evolution of pore-water pressure is given by the following equation:

$$(7) \quad \frac{dp_{wb}}{dt} = \frac{\pi^2}{4h^2} c_v p_{wb}$$

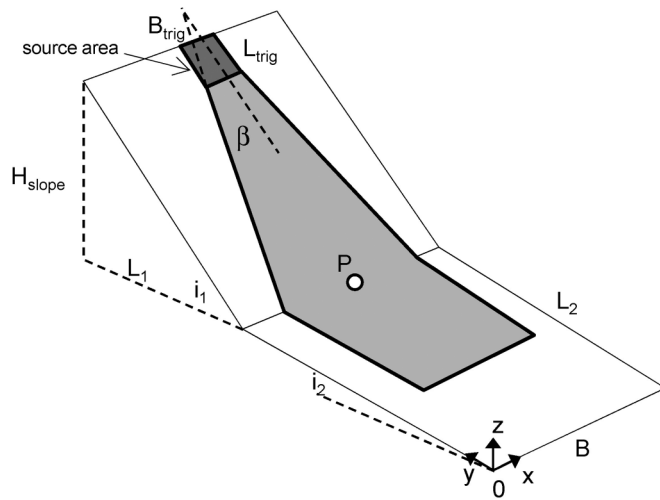
where c_v is the classical coefficient of consolidation.

The frictional model has been used extensively in the literature to investigate this type of shallow, fluidized landslide (Crosta et al. 2009; D’Agostino et al. 2013, among others), and is thus suitable for use in this paper. Indeed, the use of the frictional model should be encouraged: it may help to reduce the current gap between initiation analysis and propagation analysis, both which are still performed using different mathematical-numerical models despite their shared basis in classical concepts of soil friction and pore-water pressure. The sensitivity of the GeoFlow_SPH model is discussed by Pastor et al. (2009) in relation to frictional rheological law. The Voellmy law (McDougall and Hungr 2004; Dahl et al. 2013) and the quadratic law (Julien and Lan 1991), among others, are valuable rheological alternatives.

In the paper, it is assumed that the entrained material is similar to the body material of the landslide, such that the rheology does not significantly change along the landslide path. This is unrealistic in the case of landslides that entrain weaker material from the ground surface, such as giant debris avalanches containing rocks and boulders, which are beyond the scope of this paper. However, the assumption is acceptable in cases of debris avalanches that occur in coarse-grained soils (sands and gravels) along steep, unchannelised slopes.

The entrainment term (e_r) introduces to eq. (5) a velocity-dependent resistance component, the role of which may differ from that of the frictional-resistance term (τ_b), which is instead proportional to flow height. In addition, the entrainment term (e_r) appears in the balance equations for both mass and momentum (eqs. (3) and (5)), and is in turn dependent on both propagation height (h) and velocity (v) (eq. (1)). The kinematic variables (h and v) are strictly related to the basal-resistance term (τ_b), which also depends on the pore-pressure term (eq. (7)). The effects of pore water are taken into account by measuring the relative height of the water (h_w^{rel}), that is, the ratio of the height of the water table to the soil thickness, the relative pressure of the water (the ratio of pore-water pressure to liquefaction pressure, p_w^{rel}), and the consolidation coefficient (c_v) is used to simulate a one-dimensional consolidation process (eq. (7)).

Fig. 2. Benchmark case for parametric analysis. B , width of slope; B_{trig} , width of source area of debris avalanche; H_{slope} , height of slope; i_1, i_2 , slope angles; L_1, L_2 , length of slope; L_{trig} , length of source area of debris avalanche.



Benchmark cases

To assess the roles of entrainment, frictional basal resistance and pore-water pressure in the lateral spreading of the propagating mass, an ideal slope is parametrically analysed. The slope consists of two planes with inclines to the horizon of i_1 and i_2 (Fig. 2). The failed volume is located at the uppermost edge of the upper slope, inside the so-called source area (Fig. 2) from which the material slips down. The propagation area of a debris avalanche is analysed with reference to the semi-apical angle (β) computed from the lateral boundary of the debris avalanche to its axis at the source area. Other important features, such as the angle of reach (α) formed by the line connecting the uppermost point of the landslide crown scarp to the distal boundary of the mass deposit in a longitudinal section, are not investigated here, as they also depend on piedmont characteristics (Cascini et al. 2011a).

First, a material with a zero friction angle and a unit weight of 10 kN/m^3 is modelled to analyse the ideal case of a water-like material moving along an open slope (Table 1). Figure 3 clearly shows that with a sufficiently small slope angle, the transversal and longitudinal velocities of the propagating mass will be approximately equal and the semi-apical angle (β) will approach 90° ; larger slope angles produce greater longitudinal propagation velocities, which exceed transversal velocity, and smaller simulated semi-apical angles. In the case of a 500 m long hillslope with a 45° steepness, the simulated semi-apical angle is about 11° . The results for fluid-like materials are also found to be independent of the dimensions (width/length) of the source area and the initial height of the material.

Several analyses of frictional-like materials are performed (Table 2) by varying the morphometric features of the hillslope ($i_1, i_2, H_{\text{slope}}$), the geometrical aspect ratio of the source area ($B_{\text{trig}}, L_{\text{trig}}, h_{\text{trig}}$), and the main rheological parameter (the friction angle of the propagating mass, ϕ_b). A fixed value for landslide growth rate (E_r) is used to account for the entrainment phenomena.

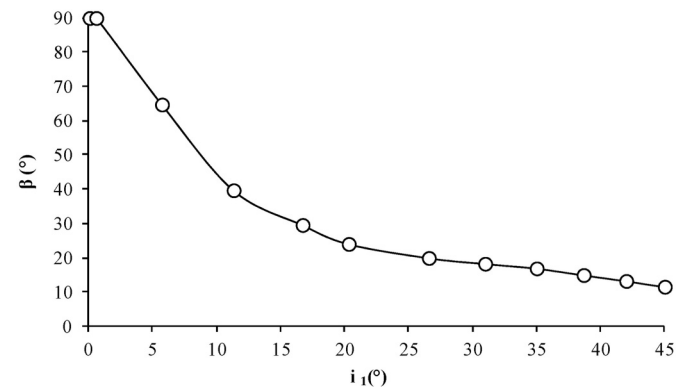
The results displayed in Fig. 4 correspond to the cases presented in Table 2, and indicate that the greater the ratio of the triggering soil height to the length of the source area ($h_{\text{trig}}/L_{\text{trig}}$), the greater the lateral spreading (β), with a maximum of 8.3° reached in case 11d. The 8.3° maximum corresponds to a triggering soil height of 5 m. Such a high h_{trig} value is likely to occur in zone 2 of the slope shown in Fig. 1 due to the impact of material falling from a bed-rock scarp. It is worth noting that the semi-apical angles (β) simulated for the frictional-like materials presented in Table 2 (Fig. 4)

Table 1. List of simulated cases for a water-like material on the benchmark slope shown in Fig. 2.

| Case | i_1 ($^\circ$) | H_{slope} (m) | L_1 (m) |
|------|--------------------|------------------------|-----------|
| a | 0.00 | 105 | 100 |
| b | 0.57 | 104 | 100 |
| c | 5.72 | 103 | 100 |
| d | 11.38 | 103 | 200 |
| e | 16.93 | 103 | 300 |
| f | 20.72 | 103 | 370 |
| g | 23.53 | 600 | 218 |
| h | 27.47 | 600 | 600 |
| i | 32.35 | 600 | 300 |
| l | 36.91 | 600 | 360 |
| m | 41.10 | 600 | 420 |
| n | 44.88 | 600 | 480 |

Note: $i_2 = 20^\circ, L_2 = 500 \text{ m}, B = 800 \text{ m}, L_{\text{trig}} = 10 \text{ m}, B_{\text{trig}} = 50 \text{ m}, h_{\text{trig}} = 2 \text{ m}$. i_1, i_2 , slope angles; L_1, L_2 , length of slope; B , width of the slope; $L_{\text{trig}}, B_{\text{trig}}$, length and width of the source area of debris avalanche, respectively; H_{slope} , height of slope; h_{trig} , initial height of soil in the source area.

Fig. 3. Simulated semi-apical angle (β) versus slope inclination (i_1) for frictionless fluid.



are in each case lower than those simulated for water-like materials (Fig. 3).

Figure 5 provides an example of these results with $L_{\text{trig}}, B_{\text{trig}}, \phi_b, c_v,$ and E_r fixed at 50 m, 40 m, 10.2° , $0.01 \text{ m}^2/\text{s}$, and $8.2 \times 10^{-3} \text{ m}^{-1}$, respectively. The semi-apical angle (β) increases from 1.3° to 5.2° until a $B_{\text{trig}}/L_{\text{trig}}$ value of 0.5 is reached, and then reduces to a minimum value of 3.2° , independent of relative pore-water pressure (p_w^{rel}) at 0.5/1.

Finally, Fig. 6 shows the time trend in simulated eroded depths for the cases in Table 2 at point P of Fig. 2, on the boundary between slope and piedmont. The final eroded depths (h_{er}) range from 1 to 10 m, with an erosion rate (e_r , defined in eq. (1)) ranging from 0.08 to 1.29 m/s (Fig. 6), and an erosion time (t_{er} , defined as the time in which bed entrainment occurs at a given point of the slope) ranging from 3.4 to 22.7 s (Fig. 6).

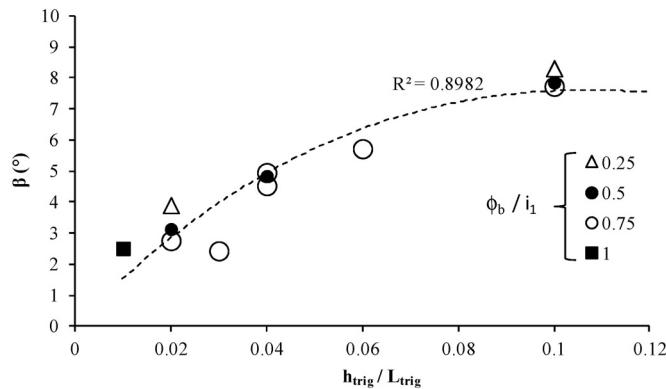
Globally, the apical angle produced by frictional materials is always lower than that produced by fluid materials. In the case of frictional materials, basal shear stress is high enough to limit lateral spreading in the x direction (corresponding to any horizontal contour line), as shown in Fig. 2, whereas the spreading of fluid materials in the x direction is only limited by the value of the flow height, which decreases as fast as the flow propagates in the y direction shown in Fig. 2 (i.e., downslope). The eroded depths simulated at the boundary between slope and piedmont show two key characteristics: (i) they are the product of a combination of slope morphology, features of the triggering area, rheology, and bed entrainment; and (ii) they range consistently between 0.03 and 10.07 m for a wide array of debris avalanches in coarse-grained

Table 2. List of simulated cases for a frictional entraining material along the benchmark slope shown in Fig. 2.

| Case | ϕ_b (°) | i_1 (°) | i_2 (°) | H_{slope} (m) | L_{trig} (m) | B_{trig} (m) | h_{trig} (m) |
|------|--------------|-----------|-----------|------------------------|-----------------------|-----------------------|-----------------------|
| 1 | 30 | 35 | 10 | 400 | 50 | 10 | 2 |
| 2 | 30 | 30 | 20 | 600 | 10 | 50 | 3 |
| 3 | 30 | 30 | 10 | 200 | 100 | 10 | 3 |
| 4 | 30 | 40 | 0 | 200 | 10 | 10 | 3 |
| 5 | 30 | 40 | 0 | 200 | 100 | 50 | 3 |
| 7 | 30 | 30 | 10 | 400 | 100 | 50 | 1 |
| 8 | 30 | 35 | 10 | 400 | 10 | 50 | 2 |
| 9 | 30 | 40 | 20 | 400 | 10 | 50 | 2 |
| 10 | 30 | 40 | 20 | 600 | 50 | 50 | 2 |
| 11a | 30 | 40 | 20 | 600 | 50 | 50 | 1 |
| 11b | 30 | 40 | 20 | 600 | 50 | 50 | 2 |
| 11c | 30 | 40 | 20 | 600 | 50 | 50 | 3 |
| 11d | 30 | 40 | 20 | 600 | 50 | 50 | 5 |
| 11e | 20 | 40 | 20 | 600 | 50 | 50 | 1 |
| 11f | 20 | 40 | 20 | 600 | 50 | 50 | 2 |
| 11g | 20 | 40 | 20 | 600 | 50 | 50 | 5 |
| 11h | 10 | 40 | 20 | 600 | 50 | 50 | 1 |
| 11i | 10 | 40 | 20 | 600 | 50 | 50 | 5 |
| 12 | 10 | 40 | 20 | 600 | 50 | 50 | 1 |
| 13a | 10 | 40 | 20 | 600 | 50 | 75 | 1 |
| 13b | 10 | 40 | 20 | 600 | 50 | 75 | 2 |
| 13c | 10 | 40 | 20 | 600 | 50 | 75 | 3 |
| 14 | 10 | 40 | 20 | 600 | 50 | 100 | 2 |
| 15 | 10 | 40 | 20 | 600 | 50 | 25 | 2 |

Note: $h_w^{\text{rel}} = 0.40$, $p_w^{\text{rel}} = 0.5$, $c_v = 0.01 \text{ m}^2/\text{s}$, $E_r = 8.2 \times 10^{-3} \text{ m}^{-1}$, $L_2 = 500 \text{ m}$, $B = 800 \text{ m}$. i_1, i_2 , slope angles; L_1, L_2 , length of slope; B , width of the slope; $L_{\text{trig}}, B_{\text{trig}}$, length and width of the source area of debris avalanche; H_{slope} , height of slope; h_{trig} , initial height of soil in the source area; ϕ_b , basal friction angle; h_w^{rel} , ratio of the height of water table to the soil thickness; p_w^{rel} , ratio of pore-water pressure to liquefaction pressure; c_v , consolidation coefficient; E_r , landslide growth rate.

Fig. 4. Simulated semi-apical angle (β) versus h_{trig} and ϕ_b (cases 11a–11i of Table 2) for frictional-like material. R^2 , coefficient of determination.



soils. Therefore, the results of the benchmark cases facilitate assessment of the roles and interplay of entrainment, rheology, and pore-water pressure, and provide theoretical values for apical angle (β), erosion rate (e_r), eroded depth (h_{er}), and erosion time (t_{er}) in highly idealized cases. Using these results, the analysis of relevant case histories in the following sections can be approached with confidence.

Case study of Campania region of southern Italy

A 3000 km² area of the Campania region of southern Italy is covered with pyroclastic soils to a thickness of 1–5 m along the slopes, originating from the explosive activity of the Somma-Vesuvius volcano (Bilotta et al. 2005). Flow-type landslides are a significant natural hazard in this area, causing frequent casualties and huge economic damage (Cascini et al. 2013b). Although sev-

Fig. 5. Simulated semi-apical angle (β) versus B_{trig} and p_w^{rel} ($i_1 = 40^\circ$, $i_2 = 20^\circ$) for frictional-like material.

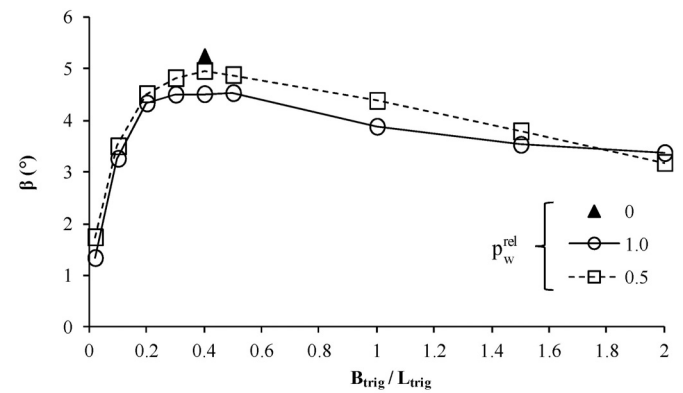
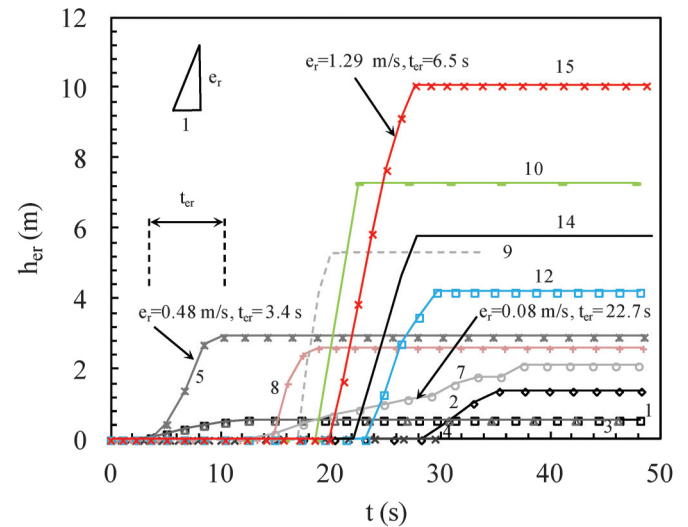


Fig. 6. Erosion depths simulated for point P in Fig. 2 (labels refer to numbering of Table 2) for frictional-like material.



eral debris avalanches have been recorded during past landslides in this area (Cascini et al. 2013b), they have not yet been fully numerically modelled in the literature (Cascini et al. 2013a) with attention to both bed entrainment and spatial-temporal variation in pore-water pressure in propagating masses.

However, extensive work has been done to characterize the mechanical properties of pyroclastic soils in stable conditions on the slopes. Pyroclastic soils have been shown to be fairly light materials, with unit soil weights of 13–15 kN/m³ and effective friction angles of 33°–39° (Bilotta et al. 2005). Cascini et al. (2010, 2013a, 2013c) offers detailed geomechanical models of the failure and post-failure stages of shallow landslides that originate in debris flows or debris avalanches in pyroclastic soils, providing evidence for the fundamental role of pore-water pressure in landslide behaviour. In addition, numerical analyses have been performed to investigate the rheology of pyroclastic soils involved in debris flows. The findings indicate that friction angle is drastically reduced (to 19°–22°) during the propagation stage, and that landslide growth rates may take a wide range of values, from 2.5×10^{-4} to $8.2 \times 10^{-3} \text{ m}^{-1}$ (Revellino et al. 2004; Pastor et al. 2009; Cascini et al. 2009, 2012). This extensive existing research is used in this paper to numerically calibrate the material rheology and the growth rate of debris avalanches, with the following caveats: (i) laboratory testing conditions for the analysis of the propagation stage (e.g., using a rheometer) are highly idealized; (ii) laboratory investigations of pyroclastic materials are still limited; and

Fig. 7. Overview of Nocera Inferiore debris avalanche (4 March 2005).



(iii) few attempts have been made to model the propagation stage of debris avalanches in pyroclastic soils (Cascini et al. 2013a).

This paper investigates three debris avalanches in the Campania region of Italy, spanning a wide variety of hillslope configurations and piedmont characteristics. The results are compared to provide overall insights into the behaviour of debris avalanches in pyroclastic soils.

Short run-out debris avalanche

The first case history examined is the Nocera Inferiore debris avalanche (4 March 2005), which was triggered at the intermediate portion (412 m above sea level (a.s.l.)) of the Monte Albino hillslope (1100 m high), spread out at a semi-apical angle (β) of about 9° and stopped at the piedmont area (100 m a.s.l.) after a propagation distance of only 500 m (Fig. 7). The peculiarities of the avalanche's propagation and deposition stages prompt the advanced numerical analysis performed here using the GeoFlow_SPH model.

A DTM comprising a mesh of 9348 $5\text{ m} \times 5\text{ m}$ squares is used to conduct the numerical analysis, with the initial mass schematized into a set of 2369 SPH computational points, 1 m spaced and with a uniform height of 1–2 m over a source area (data from Pagano 2009). The rheological parameters proposed by Pastor et al. (2009) are used; the landslide growth rate (E_r) is assumed to fall between 4.0×10^{-4} and $1.0 \times 10^{-2}\text{ m}^{-1}$; and a full parametric analysis (Table 3) is carried out to adequately simulate the observed behaviour of the landslide.

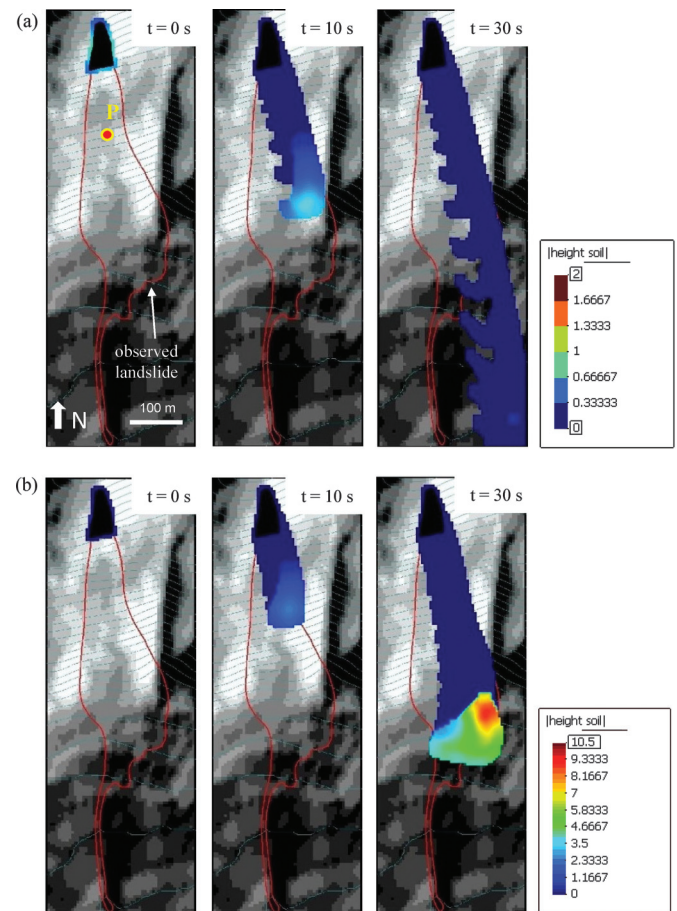
The results indicate that bed entrainment plays a major role in the whole propagation pattern (Fig. 8), as is clear from cases 7b and 7a in Table 3. In the former case, bed entrainment causes the cessation of the landslide at the piedmont, in agreement with the in situ observations; in the latter case, the landslide exhibits a much longer run-out distance, as bed entrainment is disregarded. The results shown in Fig. 8b provide a satisfactory simulation of the observed behaviour, with the exception of the lateral right-hand boundary of the debris avalanche, where it may be argued that another unstable mass was triggered. In particular, the rheological values (p_w^{rel} , c_v , h_w^{rel}) used in the best-fit case (case 7b in Table 3) are consistent with those used by Cascini et al. (2012) to back-analyse a debris flow that occurred at a similar site (Sarno), about 9 km from the study area), with the exception of the frictional angle, which is 19° in the Nocera Inferiore case and 22° as observed by Cascini et al. (2012). However, the back-analysed land-

Table 3. Simulated cases for the back-analysis of the Nocera Inferiore debris avalanche (4 March 2005).

| Case | ϕ_b ($^\circ$) | h_w^{rel} | c_v (m^2/s) | E_r (m^{-1}) |
|------|-----------------------|--------------------|---------------------------------|---------------------------|
| 0 | 22 | 0.25 | 1.11×10^{-2} | 8.2×10^{-3} |
| 1 | 22.5 | 0.25 | 1.11×10^{-2} | 8.2×10^{-3} |
| 2 | 22.5 | 0.25 | 10^{-2} | 8.2×10^{-3} |
| 4 | 22.5 | 0.40 | 10^{-2} | 8.2×10^{-3} |
| 5 | 24 | 0.40 | 10^{-2} | 8.2×10^{-3} |
| 6 | 19 | 0.40 | 10^{-2} | 8.2×10^{-3} |
| 7a | 19 | 0.40 | 10^{-2} | 0 |
| 7b | 19 | 0.40 | 10^{-2} | 8.2×10^{-3} |
| 8 | 24 | 0.40 | 10^{-2} | 8.2×10^{-3} |
| 9 | 22 | 0.10 | 10^{-2} | 10^{-2} |
| 10 | 22 | 0.10 | 10^{-3} | 10^{-2} |

Note: $p_w^{\text{rel}} = 1.0$.

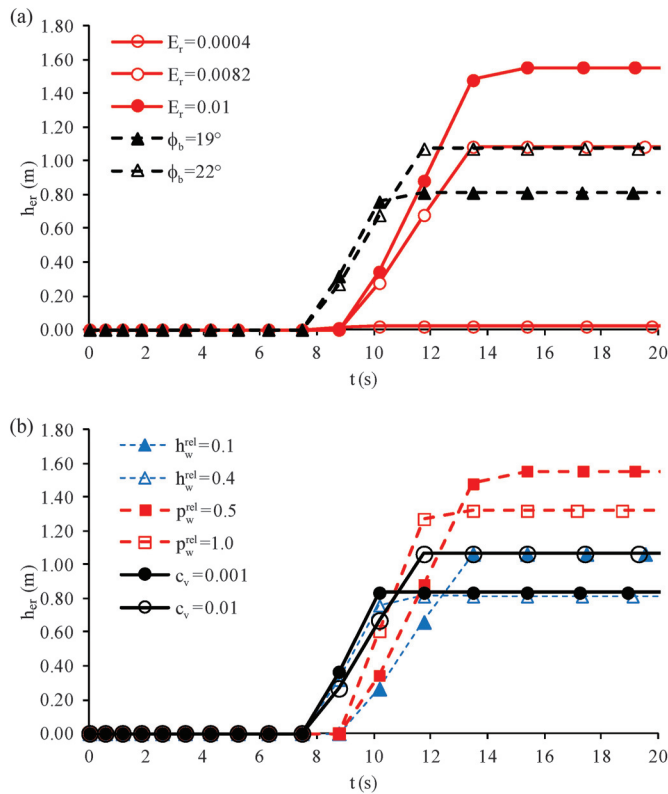
Fig. 8. Results for (a) case 7a and (b) case 7b of Table 3 compared with in situ evidence.



slide growth rate for Nocera Inferiore is $8.2 \times 10^{-3}\text{ m}^{-1}$, which is consistent with the rates observed by Cascini et al. (2012, 2013a) for similar landslides in Sarno. Due to the high value of E_r , the simulated erosion heights attain 4 m at the piedmont area of the hillslope, where the simulated soil heights reach up to 10 m, thus causing the abrupt cessation and deposition of the propagating mass.

Figure 9 is designed to clarify the understanding of the landslide's behaviour. It shows the simulated eroded heights (h_{er}) for a representative point (point P in Fig. 8) at the lowest part of the hillslope, close to the piedmont boundary. An increased friction angle (ϕ_b) is found to increase the simulated eroded heights. However, bed entrainment is reduced by an increase in either pore-

Fig. 9. Erosion depths simulated for point P of Fig. 8, depending on rheological and erosion parameters: (a) influence of landslide growth rate and basal friction angle; (b) influence of relative pore-water pressure and consolidation coefficient.



water pressure (p_w^{rel}) or the relative height of the water (h_w^{rel}). An increased consolidation coefficient (c_v) is analogous to an increased friction angle because basal shear stress increases as soon as pore-water pressure dissipates. In all of the cases under study, the eroded heights range from 0.6 to 1.60 m, in agreement with in situ observations of these events. In the best-fit case, the simulated erosion rate of the 2005 debris avalanche (e_r) is 0.23 m/s, and the simulated erosion time (t_{er}) is 4.7 s, which are both consistent with the results achieved for the benchmark case discussed in the section “Benchmark cases”. Finally, it is interesting to note that satisfactory results cannot be obtained by increasing the basal resistance (e.g., frictional angle) without considering entrainment. In fact, entrainment introduces into eq. (5) a velocity-dependent resistance component that increases as the unstable mass travels along the slope and approaches the piedmont zone; in contrast, frictional resistance is only related to flow height, which diminishes as the debris avalanche propagates downslope due to lateral spreading.

Debris avalanche bifurcated into two debris flows

Unlike the previous case, a debris avalanche may be triggered at the uppermost part of a hillslope, and unstable material may propagate into a well-established channel or even spread into two or more valleys. The latter case was recorded on 5 May 1998 at the Pizzo d’Alvano massif (about 1000 m high), in the Cortadonica basin. A debris avalanche was triggered at 745 m a.s.l., enlarged along the hillslope at a semi-apical angle (β) of about 7° , travelled for 510 m, then divided in two wide valleys. It propagated over a total run-out distance of 1.95 km up to the piedmont area at 65 m a.s.l. (Fig. 10).

The numerical analysis of this case (Table 4) is performed using a $3\text{ m} \times 3\text{ m}$ DTM from which a topographic mesh of 35 520 squares

Fig. 10. Aerial view of debris avalanche that occurred at Sarno (Cortadonica basin, 5 May 1998).

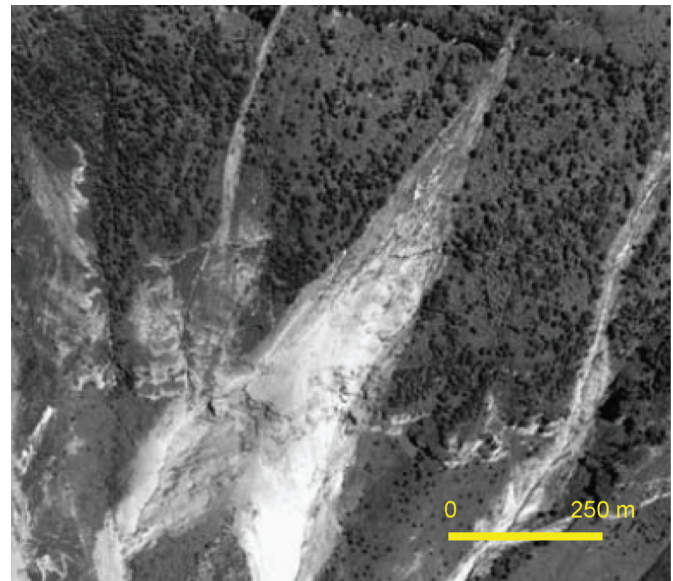


Table 4. Simulated cases for the back-analysis of a debris avalanche at Sarno (Cortadonica basin, 5 May 1998).

| Case | ϕ_b ($^\circ$) | h_w^{rel} | E_r (m^{-1}) |
|----------------|-----------------------|-------------|---------------------------|
| 0 | 22 | 0.25 | 1.2×10^{-4} |
| 1 | 22.5 | 0.25 | 1.2×10^{-4} |
| 2 | 22.5 | 0.25 | 1.2×10^{-4} |
| 3 | 22.5 | 0.25 | 4.0×10^{-4} |
| 4 | 22.5 | 0.40 | 4.0×10^{-4} |
| 5 | 24 | 0.40 | 4.0×10^{-4} |
| 6 ₁ | 22.5 | 0.10 | 4.0×10^{-4} |
| 6 ₂ | 19 | 0.40 | 4.0×10^{-4} |
| 7 ₁ | 22.5 | 0.25 | 1.2×10^{-4} |
| 7 ₂ | 19 | 0.40 | 8.2×10^{-3} |
| 8 | 19 | 0.25 | 1.2×10^{-4} |
| 9 | 24 | 0.25 | 1.2×10^{-4} |
| 10 | 22.5 | 0.25 | 8.2×10^{-3} |
| 11 | 22.5 | 0.25 | 2.0×10^{-3} |
| 12a | 22.5 | 0.25 | 0 |
| 12b | 22.5 | 0.25 | 4.0×10^{-4} |
| 13 | 22.5 | 0.25 | 3.0×10^{-3} |

Note: $p_w^{rel} = 1.0$; $c_v = 0.01\text{ m}^2/\text{s}$.

is derived. The initial mass is schematized into a set of 639 SPH points, 1 m spaced, with a uniform soil height of 1–2 m over the impact zone (data from Cascini et al. 2005, 2008). A frictional model is used to analyse the rheological behaviour of the unstable mass, based on the rheological parameters used by Pastor et al. (2009) to back-analyse an important channelised landslide that occurred during the May 1998 event in a neighbouring mountain basin. The landslide growth rate is assumed to range from 1.3×10^{-4} to $8.2 \times 10^{-2}\text{ m}^{-1}$, which is similar to the rate of the Nocera Inferiore landslide, due to important similarities between either morphometric hillslope features or soil mechanical parameters in the two areas under study (Cascini et al. 2013a).

The results shown in Fig. 11b provide a satisfactory simulation of the observed behaviour of the landslide, especially in terms of the lateral boundary of the debris avalanche and the splitting of its initial mass into two channels. The estimated landslide growth rate is $4.0 \times 10^{-3}\text{ m}^{-1}$, which is half of the value estimated for the Nocera landslide. Moreover, the rheological parameters (case 12 of Table 4) closely match those found by Cascini et al. (2012), with the

Fig. 11. Results achieved for (a) case 12a and (b) case 12b of Table 4 compared with in situ evidence.

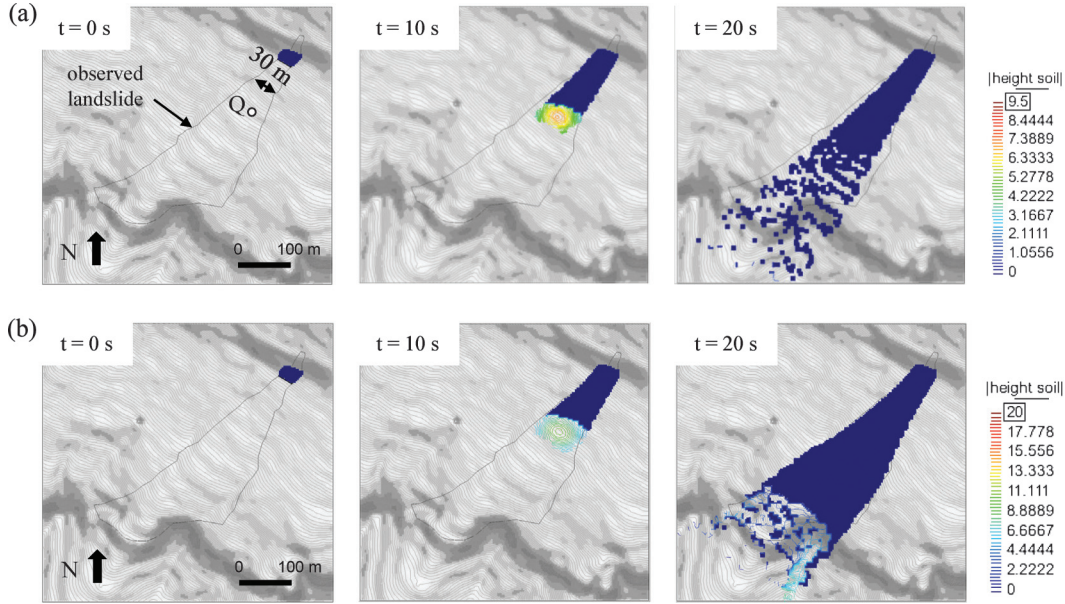
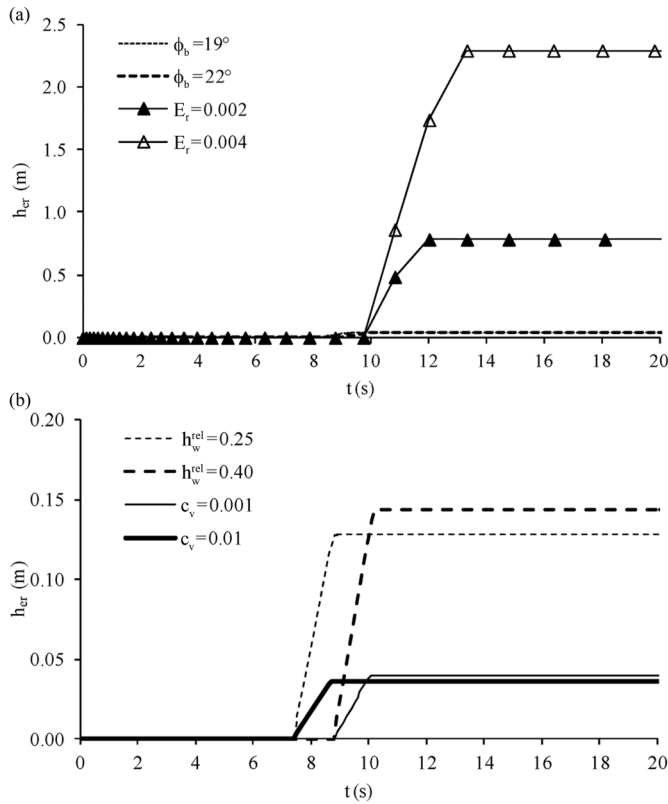


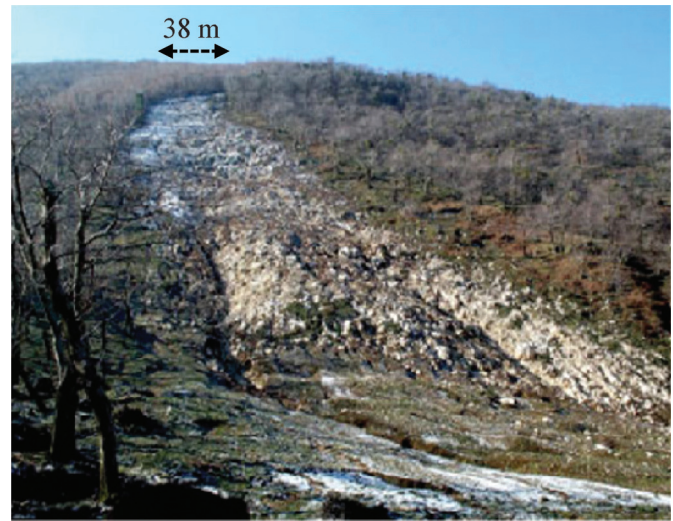
Fig. 12. Erosion depths simulated for point Q of Fig. 11, depending on rheological and erosion parameters: (a) influence of landslide growth rate and basal friction angle; (b) influence of relative pore-water pressure and consolidation coefficient.



exception of minor differences in the frictional angle and consolidation coefficient (c_v). The simulated erosion rate (e_r) is 0.57 m/s, and the simulated erosion time (t_{er}) is 2.5 s. These values are quite similar to the equivalent measurements at Nocera.

All of the results achieved for the Cortadonica debris avalanche show that the greater the friction angle (Fig. 12a) or erosion

Fig. 13. Overview of Cervinara debris avalanche, which occurred on 15 December 1999 (Damiano 2003).



growth rate (Fig. 12b), the higher the simulated eroded heights (h_{er}); similarly, if the consolidation coefficient (c_v) increases, the depth of erosion increases (Fig. 12a). These results are shown in Fig. 12, with reference to the simulated erosion height (h_{er}) of a representative point (point Q in Fig. 11) in the middle of the debris-avalanche source area. Moreover, it is shown that bed entrainment (Fig. 12b) decreases if the water-table height increases (h_w^{rel}). These results are consistent with those obtained for the previous case history.

Debris avalanche with complex propagation pattern

The Cervinara site (Ioffredo Basin, 15 December 1999) provides a representative example of a debris avalanche evolving into a debris flow (Fig. 13). The Cervinara debris avalanche (Damiano 2003; Olivares and Picarelli 2003; Cascini et al. 2011b) was triggered at 720 m a.s.l., enlarged along the hillslope at a semi-apical angle (β) of about 7°, travelled over a distance of 360 m and fell into a valley. It propagated over a total run-out distance of 1.4 km up to the piedmont area at 302 m a.s.l. (Fig. 14).

Fig. 14. Results achieved for (a) case 19a and (b) case 19b of Table 5 compared with in situ evidence.

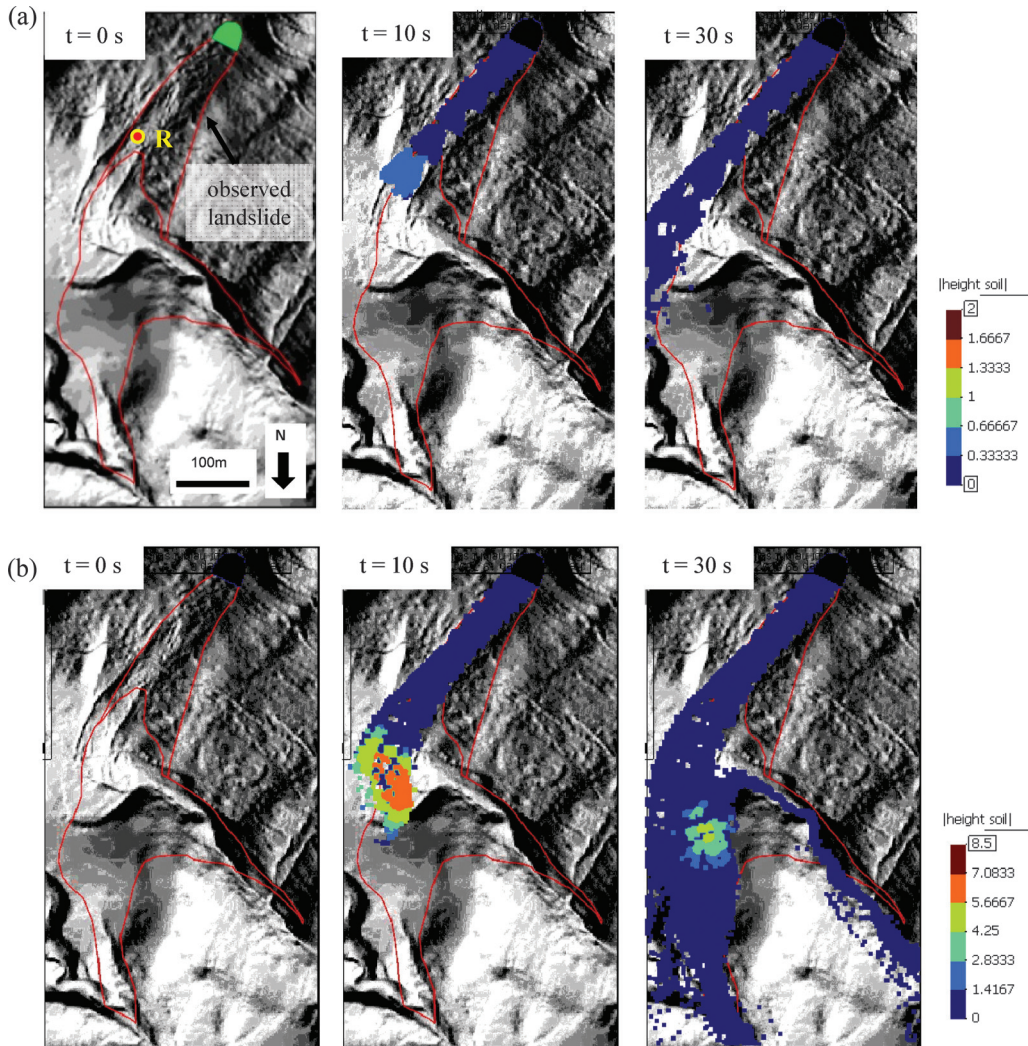


Table 5. Simulated cases for the back-analysis of the Cervinara debris avalanche (15 December 1999).

| Case | ϕ_b (°) | h_w^{rel} | E_r (m ⁻¹) |
|------|--------------|-------------|--------------------------|
| c | 15 | 0.10 | 0.010 |
| i | 15 | 0.10 | 0.010 |
| f | 24 | 0.10 | 0.010 |
| 11 | 22.5 | 0.25 | 0.002 |
| 12 | 22.5 | 0.25 | 0.004 |
| 13 | 22.5 | 0.25 | 0.003 |
| 19a | 9 | 0.40 | 0 |
| 19b | 9 | 0.40 | 0.010 |

Note: $p_w^{rel} = 1.0$; $c_v = 0.01$ m²/s.

The numerical analyses of this avalanche are performed using a 2 m × 2 m DTM, giving a topographic mesh of 62 282 squares (Fig. 14). All of the analyses refer to a set of 1600 SPH computational points, 1 m spaced and characterized by a uniform height of 2–4 m inside the source zone (data from Cascini et al. 2011b). The entrainment rate is assumed to range from 2.0×10^{-3} to 1.0×10^{-2} m⁻¹, and Table 5 lists various combinations of friction angle (ϕ_b) and pore-water pressure (p_w^{rel}) according to distinct assumptions regarding the soil water-table height in the debris-avalanche source area.

Fig. 15. Erosion depths simulated for point R of Fig. 14, depending on rheological and erosion parameters.

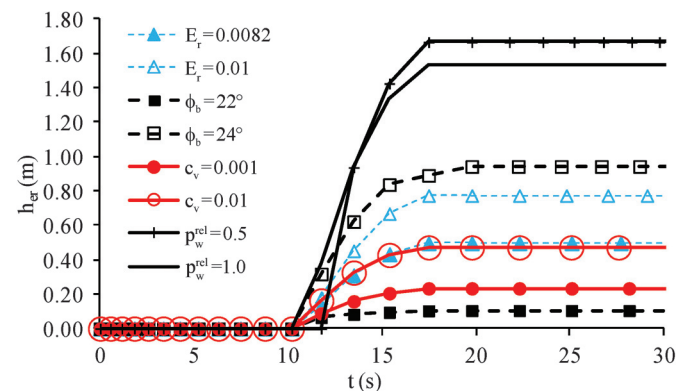


Figure 14 provides a detailed simulation of the in situ evidence (case 19 of Table 5), reproducing the typical triangular propagation zone, the run-up on the opposite slope and the final division of the propagating mass into two branches, which caused a debris flow in the larger valley and a small flow-type landslide in the smaller valley. This behaviour is simulated by dividing the topography in two parts: in the upper part, from 720 to 510 m a.s.l., E_r is

Table 6. Comparison of the results obtained for the three case histories.

| Landslide | Case | $\tan(\phi_b)$ | h_w^{rel} | p_w^{rel} | c_v (m^2/s^{-1}) | E_r hillslope (m^{-1}) | E_r channel (m^{-1}) | E_r piedmont (m^{-1}) | β ($^\circ$) | e_r (m/s) | t_{er} (s) |
|--------------------------------|---|----------------|--------------------|--------------------|---|--|--------------------------------------|---------------------------------------|----------------------|-------------|--------------|
| This paper (debris avalanches) | Benchmark (fluid-like material) | — | — | 1.0 | — | — | — | — | 11/90 | — | — |
| | Benchmark (frictional-like material) | 0.35/0.57 | 0.40 | 1.0 | 1.0×10^{-2} | 8.2×10^{-3} | — | 0 | <8 | 0.08/1.29 | 3.4/22.7 |
| | Nocera Inferiore (2005) | 0.35 | 0.40 | 1.0 | 1.0×10^{-2} | 8.2×10^{-3} | — | 8.2×10^{-3} | 9 | 0.23 | 4.7 |
| | Sarno (1998) | 0.41 | 0.25 | 1.0 | 1.0×10^{-2} | 4.0×10^{-3} | — | — | 7 | 0.57 | 2.5 |
| | Cervinara (1999) | 0.15/0.35 | 0.40 | 1.0 | 1.0×10^{-2} | 4.0×10^{-3} | — | 0 | 7 | 0.11 | 5.71 |
| Debris avalanches | Cascini et al. (2013a) | 0.40 | 0.25 | 1.0 | 1.1×10^{-2} (1.2×10^{-3})/ (8.2×10^{-3}) | — | — | — | 7 | — | — |
| Flowslides | Pastor et al. (2009) | 0.4 | 0.25 | 1.0 | 1.1×10^{-2} | — | — | — | — | — | — |
| | Cascini et al. (2012) | 0.35/0.40 | 0.4 | 1.0 | 1.0×10^{-2} | — | 4.0×10^{-4} | 0 | — | — | — |

Note: —, not considered or not defined.

assumed to be $1.0 \times 10^{-2} \text{ m}^{-1}$, while in a flatter area at the toe of the hillslope, from 510 to 430 m a.s.l., a zero landslide growth rate is assumed. The simulated erosion rate (e_r) is 5.71 m/s and the simulated erosion time (t_{er}) is 2.5 s.

In addition, Fig. 14 shows the simulated erosion height (h_{er}) of a representative point (point R in Fig. 15) at the middle section of the landslide. The eroded heights significantly increase if the friction angle or the consolidation coefficient (c_v) increases; however, the bed entrainment may also increase due to a reduction in pore-water pressure (p_w^{rel}) or water-table height (h_w^{rel}).

The Cervinara debris avalanche (similar to the Sarno and Nocera Inferiore avalanches) shows a higher landslide growth rate (Table 6) than other debris flows occurring in the same region. In Table 6, an overview is given of the erosion rates (e_r) and erosion times (t_{er}) computed for both the benchmark cases and the case studies under analysis. Investigating both of these sets of values may provide useful strategies for formulating and testing more accurate physical laws for bed entrainment, which is one of the key factors determining the behaviour of debris avalanches.

Concluding remarks

In this paper, the propagation stage of debris avalanches is numerically modelled. Debris avalanches have important and distinctive features, as they involve open slopes and affect triangular source areas in which initial slides spread out and turn into avalanches. In a novel contribution to the literature, the simulations in this paper accommodate the effects of pore-water pressure as an independent variable changing in space and time, via a one-dimensional consolidation process during the propagation stage. In addition, bed entrainment is investigated by testing the simplified hypothesis — applicable to the class of phenomena investigated — that rheology is independent of entrainment. Therefore, the results offer valuable new insights into the behaviour of debris avalanches by providing a wide range of scenarios for comparison with the debris avalanches observed, simulated, and discussed in the existing literature.

The results of the benchmark tests show that the semi-apical angle (β) of a debris avalanche depends on the material type, slope inclination, and geometric aspect ratio of the source area. In the case of water-like materials (i.e., with a zero friction angle), an increased slope inclination reduces the semi-apical angle because the material propagates to a greater degree along the slope than it spreads laterally. In particular, the semi-apical angle for a 45° hillslope is 11° , which could be considered an upper limit for debris avalanches involving completely liquefied materials and characterized by a negligible entrainment rate. Conversely, if bed entrainment occurs, either water or solid particles are mobilized, and frictional shear resistance reduces the lateral spreading of the propagating mass. However, a mixture of water and solid grains may also entrain a significant amount of bed material, slowing down the front of the debris avalanche and contributing to the

lateral spreading of the landslide. In a novel contribution to existing research, these two relevant and contrasting mechanisms are analysed parametrically in this paper by varying the slope geometry, features of the source areas, material rheology, and entrainment features. In the cases analysed, the maximum semi-apical angle (β) is found to be about 8° . Furthermore, the final eroded depths (h_{er}) are between 1 and 10 m, with an erosion rate (e_r) ranging from 0.08 to 0.91 m/s and an erosion time (t_{er}) ranging from 10.3 to 37.6 s.

Also addressed in this paper are three important case histories drawn from the Campania region of Italy (Cervinara, Nocera Inferiore, and Sarno), which provide examples of debris avalanches in pyroclastic soils that had not previously been back-analysed through numerical modelling. The results show that debris avalanches can be adequately simulated with water pressures similar to those used in back-analysis of certain debris flows occurring in the same regions and with lower or similar friction angles. In all of the case studies considered, the simulated erosion depths are highly consistent with the in situ evidence.

This research makes a major contribution to the existing literature in showing that landslide propagation depends on the interplay of rheology and bed entrainment. It also shows that simulated eroded heights increase with either friction angle (ϕ_b) or consolidation coefficient (c_v), both of which amplify the basal shear resistance. For the same reason, an increase in pore-water pressure (p_w^{rel}) or the relative height of the water (h_w^{rel}) — corresponding to a reduction in basal shear resistance — reduces bed entrainment. However, pore-water pressure has only a minor role in the lateral spreading of debris avalanches, causing only moderate changes in apical angle.

As a whole, the results obtained confirm the efficacy of the chosen SPH depth-integrated coupled model in simulating the propagation stage of debris avalanches while taking into account the roles of soil rheology and erosion phenomena. Limitations of the present work rely on the simplifying assumptions that are encoded in the model (i.e., natural volume growth during entrainment and depth-integration of pore-water pressure), which certainly deserve further investigation.

Acknowledgement

This paper is dedicated to the memory of the recently departed Giuseppe Sorbino, whose vitality, optimism, and many other contributions to science and society will be very much missed.

References

- Bilotta, E., Cascini, L., Foresta, V., and Sorbino, G. 2005. Geotechnical characterisation of pyroclastic soils involved in huge flowslides. *Geotechnical and Geological Engineering*, 23: 365–402. doi:10.1007/s10706-004-1607-3.
- Blanc, T., Pastor, M., Drempetic, M.S.V., and Haddad, B. 2011. Depth integrated modelling of fast landslides propagation. *European Journal of Environmental and Civil Engineering*, 15: 51–72. doi:10.1080/19648189.2011.9695304.
- Bowman, E.T., Take, W.A., Rait, K.L., and Hann, C. 2012. Physical models of rock

- avalanche spreading behaviour with dynamic fragmentation. *Canadian Geotechnical Journal*, **49**(4): 460–476. doi:10.1139/t2012-007.
- Calvetti, F., Crosta, G., and Tatarella, M. 2000. Numerical simulation of dry granular flows: from the reproduction of small-scale experiments to the prediction of rock avalanches. *Rivista Italiana di Geotecnica*, **2**: 21–38.
- Cascini, L. 2004. The flowslides of May 1998 in the Campania region, Italy: the scientific emergency management. *Italian Geotechnical Journal*, **2**: 11–44.
- Cascini, L. 2005. La gestione scientifica dell'emergenza idrogeologica del maggio 1998 nella Regione Campania. Soveria Mannelli. Rubbettino, pp. 278. [In Italian.] ISBN: 88-498-0964-6.
- Cascini, L., Guida, D., and Sorbino, G. 2005. Il Presidio Territoriale. Una esperienza sul campo. Soveria Mannelli. Rubbettino. [In Italian.] ISBN: 88-498-0962-X.
- Cascini, L., Cuomo, S., and Guida, D. 2008. Typical source areas of May 1998 flow-like mass movements in the Campania region, Southern Italy. *Engineering Geology*, **96**: 107–125. doi:10.1016/j.enggeo.2007.10.003.
- Cascini, L., Cuomo, S., Ferlisi, S., and Sorbino, G. 2009. Detection of mechanisms for destructive landslides in Campania region – southern Italy. In *Proceedings of the First Italian Workshop on Landslides (IWL 2009)*, Napoli, Italy, 8–10 June 2009. Edited by L. Picarelli, P. Tommasi, G. Urciuoli, and P. Versace. pp. 43–51. ISBN: 978-88-89972-12-0.
- Cascini, L., Cuomo, S., Pastor, M., and Sorbino, G. 2010. Modelling of rainfall-induced shallow landslides of the flow-type. *Journal of Geotechnical and Geoenvironmental Engineering*, **136**(1): 85–98. doi:10.1061/(ASCE)GT.1943-5606.0000182.
- Cascini, L., Cuomo, S., and Della Sala, M. 2011a. Spatial and temporal occurrence of rainfall-induced shallow landslides of flow type: A case of Sarno-Quindici, Italy. *Geomorphology*, **126**(1–2): 148–158. doi:10.1016/j.geomorph.2010.10.038.
- Cascini, L., Cuomo, S., and De Santis, A. 2011b. Numerical modelling of the December 1999 Cervinara flow-like mass movements (Southern Italy). In *Proceedings of the 5th International Conference on Debris-Flow Hazards Mitigation: Mechanics, Prediction and Assessment*. Italian Journal of Engineering Geology and Environment, pp. 635–644. doi:10.4408/IJEGE.2011-03.B-069.
- Cascini, L., Cuomo, S., Pastor, M., Sorbino, G., and Piciullo, L. 2012. Modeling of propagation and entrainment phenomena for landslides of the flow type: the May 1998 case study. In *Proceedings of the 11th International Symposium on Landslides: Landslides and Engineered Slopes*, Banff, Alta., 3–8 June 2012, Edited by E. Eberhardt, C. Froese, K. Turner, and S. Leroueil, pp. 1723–1729. ISBN: 978-0-415-62423-6.
- Cascini, L., Cuomo, S., and Pastor, M. 2013a. Inception of debris avalanches: remarks on geomechanical modelling. *Landslides*, **10**(6): 701–711. doi:10.1007/s10346-012-0366-0.
- Cascini, L., Sorbino, G., Cuomo, S., and Ferlisi, S. 2013b. Seasonal effects of rainfall on the shallow pyroclastic deposits of the Campania region (southern Italy). *Landslides*, April: 1–14. doi:10.1007/s10346-013-0395-3.
- Cascini, L., Cuomo, S., Pastor, M., and Sacco, C. 2013c. Modelling the post-failure stage of rainfall-induced landslides of the flow type. *Canadian Geotechnical Journal*, **50**(9): 924–934. doi:10.1139/2012-0375.
- Catalano, E., Chareyre, B., Cortis, A., and Barthélémy, E. 2011. A pore-scale hydro-mechanical coupled model for geomaterials. In *Particles 2011: II International Conference on Particle-Based Methods*. Edited by E. Oñate and D.R.J. Owen. pp. 798–809.
- Catalano, E., Chareyre, B., and Barthélémy, E. 2014. Pore-scale modeling of fluid-particles interaction and emerging poromechanical effects. *International Journal for Numerical and Analytical Methods in Geomechanics*, **38**(1): 51–71. doi:10.1002/nag.2198.
- Chen, H., Crosta, G.B., and Lee, C.F. 2006. Erosional effects on runout of fast landslides, debris flows and avalanches: a numerical investigation. *Géotechnique*, **56**(5): 305–322. doi:10.1680/geot.2006.56.5.305.
- Costa, J.E., and Williams, G.P. 1984. Debris-flow dynamics. [Videotape]. U.S. Geological Survey. Open File Report 84–606.
- Crosta, G.B., Imposimato, S., and Roddeman, D.G. 2006. Continuum numerical modelling of flowlike landslides. In *Landslides from massive rock slope failure*. Edited by S.G. Evans, G. Scarascia Mugnozza, A. Strom, and R.L. Hermanns. Springer, Berlin. pp. 211–232.
- Crosta, G.B., Imposimato, S., and Roddeman, D. 2009. Numerical modelling of entrainment/deposition in rock and debris-avalanches. *Engineering Geology*, **109**(1–2): 135–145. doi:10.1016/j.enggeo.2008.10.004.
- Cuomo, S., Pastor, M., Vitale, S., and Cascini, L. 2013. Improvement of irregular DTM for SPH modelling of flow-like landslides. In *Proceedings of the XII International Conference on Computational Plasticity. Fundamentals and Applications (COMPLAS XII)*, Barcelona, Spain, 3–5 September 2013. Edited by E. Oñate, D.R.J. Owen, D. Peric, and B. Suárez. pp. 1–10. ISBN: 978-84-941531-5-0.
- Daerr, A., and Douady, S. 1999. Two types of avalanche behaviour in granular media. *Nature*, **399**: 241–243. doi:10.1038/20392.
- D'Agostino, V., Bettella, F., and Cesca, M. 2013. Basal shear stress of debris flow in the runout phase. *Geomorphology*, **201**: 272–280. doi:10.1016/j.geomorph.2013.07.001.
- Dahl, M.P., Gauer, P., Kalsnes, B.G., Mortensen, L.E., Jensen, N.H., and Veihe, A. 2013. Numerical runout simulation of debris avalanches in the Faroe Islands, North Atlantic Ocean. *Landslides*, **10**(5): 623–631. doi:10.1007/s10346-012-0355-3.
- Damiano, E. 2003. Meccanismi di innesco di colate di fango in terreni piroclastici. Ph.D. thesis dissertation. Seconda Università di Napoli. [In Italian.]
- Di Crescenzo, G., and Santo, A. 2005. Debris slides-rapid earth flows in the carbonate massifs of the Campania region (Southern Italy): morphological and morphometric data for evaluating triggering susceptibility. *Geomorphology*, **66**: 255–276. doi:10.1016/j.geomorph.2004.09.015.
- Egashira, S., Itoh, T., and Takeuchi, H. 2001a. Transition mechanism of debris flows over rigid bed to over erodible bed. *Physics and Chemistry of the Earth, Part B: Hydrology, Oceans and Atmosphere*, **26**(2): 169–174. doi:10.1016/S1464-1909(00)00235-5.
- Egashira, S., Hondab, N., and Itoh, T. 2001b. Experimental study on the entrainment of bed material into debris flow. *Physics and Chemistry of the Earth, Part C: Solar, Terrestrial & Planetary Science*, **26**(9): 645–650. doi:10.1016/S1464-1917(01)00062-9.
- Fannin, R.J., and Wise, M.P. 2001. An empirical-statistical model for debris flow travel distance. *Canadian Geotechnical Journal*, **38**(5): 982–994. doi:10.1139/t01-030.
- Hungr, O. 1995. A model for the runout analysis of rapid flow slides, debris flows, and avalanches. *Canadian Geotechnical Journal*, **32**(4): 610–623. doi:10.1139/t95-063.
- Hungr, O., and McDougall, S. 2009. Two numerical models for landslide dynamic analysis. *Computers & Geosciences*, **35**: 978–992. doi:10.1016/j.cageo.2007.12.003.
- Hungr, O., Evans, S.G., Bovis, M.J., and Hutchinson, J.N. 2001. A review of the classification of landslides of the flow type. *Environmental and Engineering Geoscience*, **7**(3): 221–238.
- Hungr, O., McDougall, S., Wise, M., and Cullen, M. 2008. Magnitude–frequency relationships of debris flows and debris avalanches in relation to slope relief. *Geomorphology*, **96**: 355–365. doi:10.1016/j.geomorph.2007.03.020.
- Hungr, O., Leroueil, S., and Picarelli, L. 2014. The Varnes classification of landslide types, an update. *Landslides*, **11**(2): 167–194. doi:10.1007/s10346-013-0436-y.
- Hutchinson, J.N. 1986. A sliding-consolidation model for flow slides. *Canadian Geotechnical Journal*, **23**(2): 115–126. doi:10.1139/t86-021.
- Iverson, R.M. 2012. Elementary theory of bed-sediment entrainment by debris flows and avalanches. *Journal of Geophysical Research*, **117**(F3): 1–7. doi:10.1029/2011JF002189.
- Jamieson, B., and Stethem, C. 2002. Snow avalanche hazards and management in Canada: challenges and progress. *Natural Hazards*, **26**: 35–53. doi:10.1023/A:1015212626232.
- Julien, P.Y., and Lan, Y. 1991. Rheology of hyperconcentrations. *Journal of Hydraulic Engineering*, **117**(3): 346–353. doi:10.1061/(ASCE)0733-9429(1991)117:3(346).
- Manzella, I., and Labiouse, V. 2009. Flow experiments with gravel and blocks at small scale to investigate parameters and mechanisms involved in rock avalanches. *Engineering Geology*, **109**: 146–158. doi:10.1016/j.enggeo.2008.11.006.
- McDougall, S., and Hungr, O. 2004. A model for the analysis of rapid landslide motion across three-dimensional terrain. *Canadian Geotechnical Journal*, **41**(6): 1084–1097. doi:10.1139/t04-052.
- McDougall, S., and Hungr, O. 2005. Dynamic modelling of entrainment in rapid landslides. *Canadian Geotechnical Journal*, **42**(5): 1437–1448. doi:10.1139/t05-064.
- Naa'im, M., Naa'im-Bouvet, F., Faug, T., and Bouchet, A. 2004. Dense snow avalanche modeling: flow, erosion, deposition and obstacle effects. *Cold Regions Science and Technology*, **39**(2–3): 193–204. doi:10.1016/j.coldregions.2004.07.001.
- Olivares, L., and Picarelli, L. 2003. Shallow flowslides triggered by intense rainfalls on natural slopes covered by loose unsaturated pyroclastic soils. *Géotechnique*, **53**(2): 283–287. doi:10.1680/geot.2003.53.2.283.
- Paganò, L. 2009. The role of rainfall history on the interpretation of flow slide triggering in pyroclastic soils. In *Rainfall-induced Landslides: Mechanisms, Monitoring Techniques and Nowcasting Models for Early Warning Systems*. Proceedings of the First Italian Workshop on Landslides, Naples, Italy, 8–10 June 2009. Studio Editoriale Doppiovoce, Naples. Edited by L. Picarelli, P. Tommasi, G. Urciuoli, and P. Versace. Vol. 1, pp. 216–223.
- Pastor, M., Quecedo, M., Fernández-Merodo, J.A., Herreros, M.I., González, E., and Mira, P. 2002. Modelling tailings dams and mine waste dumps failures. *Géotechnique*, **52**: 579–591. doi:10.1680/geot.2002.52.8.579.
- Pastor, M., Quecedo, M., Gonzalez, E., Herreros, M.I., Fernandez Merodo, J.A., and Mira, P. 2004. Modelling of landslides: (II) propagation. In *Degradation and instabilities in geomaterials*. Edited by F. Darve and I. Vardoulakis. Springer Wien, New York. pp. 319–367. doi:10.1007/978-3-7091-2768-1_11.
- Pastor, M., Blanc, T., Pastor, M.J., Sanchez, M., Haddad, B., Mira, P., Fernandez Merodo, J.A., Herreros, M.I., and Drempetic, V. 2007. A SPH depth integrated model with pore pressure coupling for fast landslides and related phenomena. In *Proceedings of the 2007 International Forum on Landslides Disaster Management*. Edited by K. Ho and V. Li. ISBN: 978962-7619-30-7.
- Pastor, M., Haddad, B., Sorbino, G., Cuomo, S., and Drempetic, V. 2009. A depth-integrated, coupled SPH model for flow-like landslides and related phenomena. *International Journal on Numerical Analysis and Methods in Geomechanics*, **33**(2): 143–172. doi:10.1002/nag.705.
- Pastor, M., Manzanal, D., Fernández Merodo, J.A., Mira, P., Blanc, T., Drempetic, V., Pastor, M.J., Haddad, B., and Sánchez, M. 2010. From solids to

- fluidized soils: diffuse failure mechanisms in geostuctures with applications to fast catastrophic landslides. *Granular Matter*, **12**: 211–228. doi:10.1007/s10035-009-0152-4.
- Pielmeier, C., and Schneebeli, M. 2003. Developments in the stratigraphy of snow. *Surveys in Geophysics*, **24**(5/6): 389–416. doi:10.1023/B:GEOP.0000006073.25155.b0.
- Pirulli, M., and Pastor, M. 2012. Numerical study on the entrainment of bed material into rapid landslides. *Géotechnique*, **62**(11): 959–972. doi:10.1680/geot.10.P.074.
- Revellino, P., Hungr, O., Guadagno, F.M., and Evans, S.G. 2004. Velocity and runout simulation of destructive debris flows and debris avalanches in pyroclastic deposits, Campania region, Italy. *Environmental Geology*, **45**: 295–311. doi:10.1007/s00254-003-0885-z.
- Sánchez, M.E, Pastor, M., and Romana, M.G. 2013. Modelling of short runout propagation landslides and debris flows. *Georisk: Assessment and Management of Risk for Engineered Systems and Geohazards*, **7**(4): 250–266. doi:10.1080/17499518.2013.797824.
- Sovilla, B., and Bartelt, P. 2002. Observations and modelling of snow avalanche entrainment. *Natural Hazards and Earth System Science*, **2**(3–4): 169–179. doi:10.5194/nhess-2-169-2002.
- Viccione, G., and Bovolin, V. 2011. Simulating triggering and evolution of debris-flows with SPH. In *Proceedings of the 5th International Conference on Debris-Flow Hazards Mitigation: Mechanics, Prediction and Assessment*. Italian Journal of Engineering Geology and Environment, pp. 523–532.
- Wang, G., Sassa, K., and Fukuoka, H. 2003. Downslope volume enlargement of a debris slide-debris flow in the 1999 Hiroshima, Japan, rainstorm. *Engineering Geology*, **69**: 309–330. doi:10.1016/S0013-7952(02)00289-2.